Journal of Electroanalytical Chemistry 871 (2020) 114357

Contents lists available at ScienceDirect

Journal of Electroanalytical Chemistry

journal homepage: www.elsevier.com/locate/jelechem

The genuine *ac*-to-*dc* proton conductivity crossover of nafion and polymer dielectric relaxations as a fuel cell polarization loss

B.R. Matos

Instituto de Pesquisas Energéticas e Nucleares, IPEN-CNEN/SP, São Paulo 05508000, Brazil

ARTICLE INFO

Article history:
Received 8 April 2020
Received in revised form 7 June 2020
Accepted 7 June 2020
Available online 14 June 2020

Keywords:
Jonscher law
Ion conductivity
Non-ohmic
Non-linear
Electric double layer
Nafion

ABSTRACT

The non-ohmic behavior of Nafion electrical properties, *i. e.*, the thickness and potential dependent conductivity, was studied in the impedance, dielectric and conductivity representations with the use of a special through-plane sample-holder in a 4-probe array. Such measurements allowed identifying the genuine *ac*-to-*dc* conductivity crossover frequency in Nafion, which occurs for $f < 10^{-1}$ Hz. In addition, the minimization of the interfacial electrode/ionomer polarizations with the 4-probe setup permitted the determination of the bulk *dc* conductivity and dielectric constant of Nafion, which are $\sigma \sim 0.03$ Scm^{-1} and $\varepsilon' \sim 10^6$ ($T = 40$ °C and $RH = 100\%$), respectively. The colossal dielectric constant is shown to increase the Debye length of the electric double layer to values comparable to the membrane thickness. Therefore, the exponential increase of the proton conductivity with increasing both membrane thickness and electric potential are a result of canceling out the non-linear effects of electric double layer caused by the high dielectric permittivity of Nafion. The *ac*-to-*dc* conductivity crossover in H_2/O_2 fuel cell impedance curves takes place for $f < 10^0$ Hz and matches with the *ex situ* impedance spectroscopy study in excellent agreement, revealing a striking result: the potential dependent conductivity of Nafion requires extra fuel cell overpotential to overcome the electrode/ionomer interfacial polarization representing an additional polarization loss to polymer electrolyte fuel cells.

1. Introduction

At present, the state of understanding of the electrical properties of perfluorinated sulfonic-acid ionomers (PFSAs) supports that the *ac*-to-*dc* conductivity crossover in 2-probe measurements takes place at $f \sim 10^6$ Hz and that the *dc* proton conductivity is $\sigma \sim 0.10$ Scm^{-1} [1–8]. And likewise, considers that the dielectric constant of Nafion should be equally obtained at $f \sim 10^6$ Hz, at which the magnitude corresponds to those values found for polymers with embedded water ($\varepsilon' \sim 10^2$ units) [1–8]. In this perspective, for $f < 10^6$ Hz, the impedance (and dielectric) curve is mainly interpreted to be dominated by the electrode polarization phenomena [1–8]. However, in the 2-probe setup ionomer polarizations due to Nafion are distinguished in the spectra, which cast doubts on the origin of the low frequency portion ($f < 10^6$ Hz) of the impedance plot [9–12]. Nonetheless, the difficulty in finding the genuine *dc* conductivity of Nafion could be unequivocally solved with 4-probe impedance spectroscopy measurements. Simonsson et al., Wainright et al., Tanaka et al. and Xie et al. performed 4-probe impedance measurements in Nafion [4–6,39]. Based on in-plane (4-probe) conductivity measurements, these authors agreed that the conductivity ($\sigma \sim 0.1$ Scm^{-1}) is independent of frequency since the very high frequency limit of the impedance curve ($f < 10^5$ Hz). However, the IS measurements were performed in a limited frequency interval ($10^5 > f > 10^0$ Hz) [4–6,39], and compared to the current broad frequency range reached by IS ($10^8 > f > 10^{-3}$ Hz), the determination of the total impedance of the film may be inhibited. Furthermore, with the use of in-plane platinum wires, the high degree of electric field edge distortions do not allow representing the electric data in the dielectric formalism for a thorough characterization of the Nafion two well-defined relaxations existing in the frequency range of $f \sim 10^{-1} - 10^6$ Hz [11]. The uncertainties on the understanding of Nafion impedance/dielectric spectra in a wide frequency range reveal the need of revisiting such electrical data.

From the very beginning of the investigations of the electric/dielectric data of Nafion, no consensus was established for the correct spectral assignment in the framework of the two main existing and opposing interpretations [2–11]. Basically, the earliest report (1990) that displayed Nafion's Nyquist plot was provided by Pourcelly et al. [2]. In Pourcelly's work, the *dc* conductivity of Nafion in the acid form, as evaluated in the impedance spectra ($Z^* = Z' + iZ''$), was assigned to occur at high frequencies, $10^6 > f > 10^3$ Hz [1–8]. At a similar period (1988), the dielectric spectra analyses were pioneered provided by Mauritz et al. [11]. However, in Mauritz's work the *dc* proton conductivity, as evaluated in the dielectric spectra ($\varepsilon^* = \varepsilon' - i\varepsilon''$), was shown to take place for $f < 10^{-1}$ Hz [9–16]. Over the years, even in recent reports on dielectric and impedance spectroscopy of PFSAs such opposing interpretations coexist [7,8,13,16,31]. The

E-mail address: brmatos@usp.br..

http://dx.doi.org/10.1016/j.jelechem.2020.114357

assignment of the *ac*-to-*dc* crossover of Nafion either to the high or low frequency range will be abbreviated by HIFI (HIgh Frequency Interpretation) and LOFI (LOw Frequency Interpretation). Furthermore, due to the elevated proton transport properties of Nafion, this ionomer has been extensively investigated, and the information of the electric/dielectric properties is used not only as reference of performance, but as a reference of electric/dielectric spectra interpretation for a wide range of acid and alkaline ionomers, polyelectrolytes (*e.g.*, polystyrene sulfonate) and polymer electrolytes (*e.g.*, polybenzimidazole) [18]. Therefore, the discrepancy in the spectral assignment of PFSAs reveals a historical deficiency in the traditional understanding of impedance/dielectric spectroscopy of ion-containing polymers.

Specifically, in the impedance representation and in the 2-probe setup, Nafion electric spectrum (at $RH = 100\%$) displays a tail-like curve in which the high frequency end intercepts Z′ usually at $f \sim 10^3$ Hz (in-plane) and $f \sim 10^6$ Hz (through-plane) [22,23,28]. In this way, the low frequency end of such tail, which is typically observed in supercapacitors, is interpreted as a large capacitive effect due to electrode polarization phenomena [4–6]. On the other hand, in the dielectric spectroscopy representation ($\varepsilon^* = \varepsilon' + i\varepsilon''$), the log-log plots of ε'' *vs* f of Nafion displays a steep increase of the dielectric loss with decreasing frequency ($f < 10^{-1}$ Hz), which is typically interpreted to occur due to *dc* conductivity, as it is formally described by the permittivity loss term: $\varepsilon'' \approx \sigma_{dc}/2\pi f\varepsilon_0$ [11–15]. The magnitude of the proton conductivity is not directly obtained in the dielectric spectrum and probably for this reason it was previously undiscussed. Although unnoticed, the *dc* conductivity fitting of the dielectric loss plots evidenced an underlying conductivity within $\sigma \sim 10^{-5} - 10^{-7}$ Scm^{-1} (at 30 °C and $RH = 100\%$), which was estimated and explicitly taken into account just in more recent reports [7,15]. This evidence reveals a brutal difference of 5 orders of magnitude for the conductivity obtained by LOFI compared to the ones obtained by HIFI ($\sigma \sim 10^{-1}$ Scm^{-1} at 30 °C and $RH = 100\%$). The difference between the proton conductivity of LOFI ($\sigma \sim 10^{-5} - 10^{-7}$ Scm^{-1}) and the one obtained in the ohmic region of the fuel cell polarization curve ($\sigma \sim 10^{-2}$ Scm^{-1}) puts in doubt the LOFI assignment.

Since no consensus was reached for the *ac*-to-*dc* crossover, the exact determination of the dielectric constant of Nafion was similarly obtuse. Earlier dielectric spectroscopy reports on PFSAs was performed by Eisenberg et al. for Nafion in acid, ionic and non-ionic forms (SO_2F) [9,10]. In his work, Nafion dielectric relaxations were interpreted as segmental polymer motions (short and long-range motions of the polymer chains), and the dielectric spectra were not reported [9,10]. Mauritz et al. performed a more systematic investigation of the dielectric spectrum of Nafion, which showed that the dielectric permittivity measurements of hydrated Nafion in the $f \sim 10^1 - 10^6$ Hz exhibit at least two well-defined relaxation processes displaying colossal dielectric constant values ($\varepsilon' \sim 10^6$) [11]. Such relaxations were attributed to Maxwell-Wagner-Sillars (MWS) interfacial polarization within Nafion ionic clusters due to the difference of conductivity existing between ionic and nonionic phases [11]. In the most recent work of Mauritz's group, the dielectric relaxations observed for Nafion in the $f \sim 10^1 - 10^6$ Hz were assigned to be a result of the segmental motion of the polymer chains, rather than the MWS polarization [12].

Other spectral features observed for $T < 0$ °C made some authors to propose an alternative assignment to the dielectric spectrum of Nafion. Above $T \sim 0$ °C, the dielectric constant increases from $\varepsilon' \sim 10^1$ at $T = -23$ °C to $\varepsilon' \sim 10^4$ at $T = 4$ °C (at $f \sim 10^2$ Hz) [3,27]. Considering such giant dielectric constant values, Fontanella et al. attributed the dielectric spectra of Nafion in the acid form in the $f \sim 10^1 - 10^6$ Hz solely to electrode polarization, *i.e.*, to the interfacial polarization existing between the ionomer and the electrode [3,27]. Therefore, these authors concluded that the sharp rise in the dielectric permittivity values above $T \sim 0$ °C is an outcome of blocking electrode effects of high mobile ions in solution [3,27). In this framework, the dielectric permittivity of Nafion is obtained for $f > 10^6$ Hz and has dielectric constant values of $\varepsilon' \sim 10^2$; and for $f < 10^6$ Hz, the spectrum is dominated by electrode polarization effects (HIFI) [27]. More recently, Di Noto et al., based on the huge dielectric permittivity observed at low frequencies for Nafion, was in agreement with the electrode polarization assignment supported previously by Fontanella et al. [7]. However, although the LOFI and HIFI offered, respectively, by Mauritz et al. and Fontanella et al. are self-consistent, *i.e.*, both assignments follow basic impedance/dielectric spectral analysis [19], Di Noto's previous works offer a self-conflicting interpretation of Nafion dielectric spectra. Di Noto et al. assign the high frequency intercept ($f \sim 10^6$ Hz) to the *ac*-to-*dc* proton conductivity crossover of Nafion (HIFI), and assign the low frequency relaxations ($f < 10^6$ Hz) to either PTFE segmental polymer relaxation or the hydrophilic/hydrophobic accumulation of charges (LOFI) [7], *i.e.*, the same MWS polarization that was proposed in the earliest reports of Mauritz et al. [11]. As such, this assignment is a mixture of the assignments offered by Mauritz's and Fontanella's groups. The conflict in this assignment arises from considering the formalism of parallel-plate capacitors [19], where the *dc* conductivity is defined as the proton diffusion regime across the entire sample thickness reaching the electrode's surface, which compensates the electrode's surface charges and reduces the electric field in the sample bulk to zero. In this context, if the genuine *dc* conductivity of Nafion should be taken at $f \sim 10^6$ Hz, it would inevitably reduce the electric field in the Nafion bulk to zero for $f < 10^6$ Hz, thereby making it impossible to observe hydrophilic/hydrophobic polarizations in the sample bulk for $f < 10^6$ Hz, since there is no longer electric field for driving such bulk polarizations. From 2008 up to 2019 [7], Di Noto's group changed constantly the interpretation of the dielectric spectra of Nafion, which indicates that a sound experimental data to bring the impedance/dielectric analyses to a convergence is missing.

The point is that Eisenberg et al., Mauritz et al. and Colby et al. showed compelling evidences that the dielectric relaxations observed at low frequencies for Nafion display the characteristic features of processes occurring within the polymer bulk, thereby calling into question the HIFI [10,12,13]. Some other aspects evidence more problems on the HIFI. The investigations of the electric spectra of Nafion in several representations such as dielectric (ε*), electric modulus (M*), conductivity (σ*) and impedance (Z*), in a broad range of temperature, relative humidity, frequency and *ac vs dc* proton conductivity measurements revealed the existence of a low frequency proton transport in Nafion, suggesting that the low frequency intercept of the Nyquist plot could be associated with the genuine *ac*-to-*dc* conductivity crossover [15,21,22,26,30]. However, the main difficulty is to disentangle the reason why the proton conductivities obtained at $f \sim 10^{-1}$ Hz (LOFI) are tremendously discrepant when measured by either a 4-probe ($\sigma \sim 10^{-2}$ Scm^{-1}) or a 2-probe ($\sigma \sim 10^{-7}$ Scm^{-1}) setups; and more importantly, how it is comparable to the conductivity values as estimated in the ohmic region of the H_2/O_2 fuel cell *I-V* curve ($\sigma \sim 10^{-2}$ Scm^{-1}). This is the main purpose of this work.

Vayenas et al., through a series of reports, provided some advance to this topic and demonstrated that the proton conductivity of Nafion displays an ohmic and non-ohmic regime [24,25,28]. The non-ohmic behavior observed for Nafion is twofold: *i)* conductivity dependence on thickness; and *ii)* conductivity dependence on potential. It has been previously shown by different authors that Nafion conductivity increases with increasing the membrane thickness [25,47]. In addition, the proton conductivity measurements as a function of H_2 partial pressure (through-plane in 4-probe setup) evidenced very low proton conductivity values for Nafion ($\sigma \sim 10^{-5}$ Scm^{-1}) [25]. However, with increasing H_2 partial pressure from 0 to 100%, the proton conductivity increased from $\sigma \sim 10^{-5}$ Scm^{-1} to $\sigma \sim 10^{-3}$ Scm^{-1}, respectively [24,25]. Two types of proton conduction mechanisms were proposed in which the ohmic one occurs via the typical structural (Grotthuss) and vehicular motions of the protonic charges in aqueous medium, while the non-ohmic one was associated with proton tunneling among adjacent sulfonate groups [25]. Nonetheless, before questioning the quantum mechanical aspects of the proton transport, basic principles of electric and dielectric spectra data analysis must be firstly considered.

In order to confront LOFI and HIFI, this comprehensive report is dedicated to put together such spread out and isolated findings, revealing that the mostly used interpretation of the *dc* conductivity of Nafion (HIFI) leads to contradictions, and that the electrical characterization shown in

this work, unequivocally distinguishes several unconsidered aspects of the electric/dielectric data of Nafion. The results obtained are in partial consonance with the LOFI assignment provided by Mauritz et al. in which the *ac*-to-*dc* crossover is obtained at low frequencies; however, the assignments of Nafion dielectric relaxations are attributed to counterion polarization phenomena within the ionomer building blocks, rather than the segmental polymer relaxations. Moreover, this work is in partial agreement with the assignment provided by Vayenas et al., as the discrepancy of the extremely low proton conductivity with the conductivity values obtained in fuel cell polarization curves can be accounted for the potential dependent conductivity of Nafion; however, the results shown in this manuscript evidences that the origin of the non-ohmic behavior is due to the high polarizability of the ionomer building blocks due to the giant dielectric constant of Nafion, rather than proton tunneling effects. As such, the through-plane (2-probe) proton conductivity of Nafion increases by 5 orders of magnitude from $\sigma \sim 10^{-7}$ to 10^{-2} Scm^{-1} under an overpotential of ~ 400 - 500 mV. This finding evidences that the ionomer intrinsic polarizations represent an enormous overpotential in fuel cells, revealing a new approach for the improvement of the fuel cell performance.

2. Experimental

2.1. Sample preparation

2.1.1. Membranes with different thickness

Commercial Nafion membranes N112, N115 and Nafion 117 (EW = 1,100 g Eq^{-1}) were obtained from Dupont. Nafion membranes were obtained by the solution casting using the procedure reported elsewhere [14]. Basically, the cast Nafion (Ncast) was prepared by evaporating the water/alcohols solvents of Nafion 5wt% solution (Dupont) at 80 °C and dissolving the polymer slurry in dimethylsulfoxide (DMSO). Nafion/DMSO solution was poured in a Teflon mold, posteriorly placed in an oven at 160 °C for 5h. The membranes were post-treated by standard cleaning and activation protocols [14]. Samples were characterized in the hydrated form without previous thermal treatment to avoid morphological changes. The membranes were prepared with different thickness, ranging from 100 to 785 μm.

2.1.2. Membranes with different equivalent weight

The conversion of the membranes was performed using the methodology indicated by Dupont, which is nucleophilic substitution method consisting of immersing the precursor membrane in a solution of NaOH/DMSO/H_2O. Basically, Nafion pellets in the non-ionic form (RSO_2F - EW = 1,000 g Eq^{-1}) were used to prepare 100 μm films by hot-pressure above the polymer melting temperature (220 °C). The films were quenched in liquid N_2 to minimize recrystallization. These films were converted to SO_3Na groups by nucleophilic substitution, by immersing the films in NaOH solutions in H_2O/DMSO at 60 °C for 6h. Samples with EW in the 42252 to 889 g Eq^{-1} range were empirically determined by converting Nafion-SO_2F films with increasing the NaOH:SO_2F molar ratio from 8 to 128. The fully ionized sample has nominally EW = 1,000 g Eq^{-1}; however, as indicated by the product data sheet, the measured EW may be lower than the nominal EW value. The obtained films were then post-treated in 3% (w/w) H_2O_2 and 0.5 M H_2SO_4, with intermediate steps in H_2O to remove excess chemicals.

2.2. Sample characterization

2.2.1. Titration and FTIR

The equivalent weight (EW) of the composite membranes was determined by acid-base titration using the relation $EW = m/M\,v$; where m is the dry mass of the sample recorded after acidification treatment; M is the solution molarity; and v is the titrated volume. The membranes in the H^+ form were placed in a 1 M NaCl solution for 30 min and the proton concentration back titrated with a 0.01 M NaOH solution, standardized with potassium biphtalate.

FTIR spectra were measured at the IRIS beamline at the electron storage ring BESSY II of Helmholtz Zentrum Berlin (Fig. S1 / Supplementary Information) [29]. FTIR was measured in transmission mode using infrared synchrotron radiation in spectral region between 4000 and 400 cm^{-1} in the Bruker Vertex 70/v using a KBr beamsplitter, a DLaTGS detector and a silicon beamsplitter internal globar source. The spectra were taken at 2 cm^{-1} resolution and 32 scans were co-added. The references were taken through the empty channel inside the spectrometer sample compartment under vacuum.

2.2.2. NMR

In order to determine the relaxation times for the charge carriers existing in Nafion NMR spectroscopy measurements were performed. Measurements were carried out in a 1.4 T spectrometer, operating at 60 MHz for protons, equipped with a permanent magnet (Varian EM 360) and a Magritek Kea2 console. For the proton spin-spin relaxation time, T2, the Carr-Purcell Meiboom-Gill (CPMG) [30] sequence was employed. The length of the $\pi/2$ radiofrequency pulse was set to 16 ms, the echo time was τ: 100 ms and the number of echoes were varied between 500 and 1000. The data were processed by means of a 1D numerical Laplace inversion to obtain the T_2 distributions. In order to obtain the desired water content in the samples, membrane strips were placed at the bottom of a standard 5 mm NMR tube. A porous separator was set above the membrane strips and a small tube (2.5 mm OD) containing a saturated solution of the corresponding salt was inserted to control the humidity within the NMR tube. Then, the tubes were sealed and allowed to equilibrate over a minimum period of 1 month [30].

2.2.3. IS/DS

Impedance/dielectric spectroscopy measurements were performed with the equipment Solartron 1260 frequency response analyzer was used in the frequency (f) range of 4 mHz to 3 MHz applying an *ac* amplitude of 100 mV. The complex conductivity ($\sigma^* = 2\pi f\varepsilon_0\varepsilon^*$), electric modulus ($M^* = M' - iM''$) and dielectric permittivity ($\varepsilon^* = \varepsilon' - i\varepsilon''$) representations were used throughout this study, in which the dielectric spectra were obtained from:

$$\varepsilon^*(f) = \frac{1}{M^*(f)} = -\frac{S}{2\pi f\varepsilon_0 dZ^*(f)} \quad (1)$$

where ε' and ε'' are the real and imaginary parts of the dielectric permittivity; ε_0 is the vacuum permittivity (~ 8.854×10^{-14} Fcm^{-1}); S is the electrode active area, d is the thickness of the membrane; $|Z|$ and θ are the modulus and phase angle of impedance.

In-plane measurements using 2 and 4-probe terminals were carried out in a commercial sample holder (FuelCon® TrueXessory-PCM). Through-plane measurements using 2 and 4-probe terminals were performed in a specially designed airtight chamber with humidity and temperature control. 2-probe terminals measurements were performed by sandwiching Nafion samples with carbon cloths between stainless steel spring-load contact terminals, insulated from the chamber walls. 4-probe terminals measurements were performed with the stainless steel sample-holder shown schematically in Fig. 1. In 4-probe, current-generating electrodes (A) and the voltage-measuring probes (V) are separated thereby minimizing interfacial polarization due to electrode/ionomer electrical contact.

The proton conductivity measurements of samples was carried out by positioning the sample in the sample-holder and allowing the system to reach equilibrium at 30 °C at 100% of relative humidity for 24h. The impedance measurements with applied *dc* bias was performed in the frequency (f) range of 4 mHz to 3 MHz applying an *ac* amplitude of 5 - 10 mV and a *dc* amplitude in the 0 – 1100 mV range. The conductivity values obtained by impedance spectroscopy are reported to have a 10% error.

2.2.4. SAXS

SAXS experiments were carried out using synchrotron radiation at the SAXS beamline of the Brazilian National Synchrotron Light Laboratory

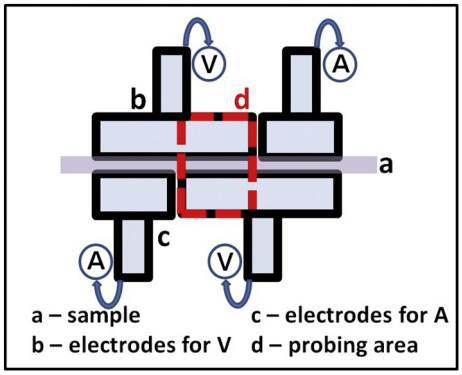

Fig. 1. Schematic representation of the through-plane setup using 4-probe stainless steel terminals. Indicated by the dashed arrow is the effective probing area.

(LNLS). Experiments were conducted with an incident wavelength $\lambda = 1.488$ Å in the range of the scattering vector $q \sim 0.02$–0.35 Å^{-1} ($q = 4\pi \sin\theta/\lambda$, with 2θ being the scattering angle). SAXS measurements of wet samples were performed by equilibrating Nafion with deionized water and then blotting the surface water with a filter paper and then enveloping it with Kapton films to prevent water evaporation during experiments. Scattering patterns were collected with MarCCD detector and the intensity curves corrected for parasitic scattering, integral intensity, and sample absorption.

2.2.5. AFM

Atomic force microscopy (AFM) experiments were carried out on an Agilent AFM/SPM Series 5500 in ACAFM microscope in contact mode. A sharp silicon beam-deflection cantilever was used. Observations were conducted on multiple areas to confirm both the uniformity and the reproducibility of the encountered experimental conditions. AFM topology images were obtained at 25 °C for annealed Nafion samples. Rectangular films were cut respecting the extrusion direction (machine direction) and positioned vertically in the substrate surface.

2.2.6. Fuel cell tests

Nafion 112 and Nafion 115 were evaluated in 5 cm^2 single fuel cell. Fuel cell tests were performed using Evaluator-C (FuelCon AG). The electrode membrane assembly (MEA) was prepared by hot pressing the prepared Nafion films with carbon cloth painted catalyst ink (Teflon + Vulcak XC 72R). The catalyst ink composition was prepared with 0.4 mg Pt cm^{-2} (Pt/C catalyst - BASF) loadings at both anode and cathode. The fuel cell were fed with pure hydrogen and oxygen at ambient pressure, $T = 80$ °C and $RH = 100\%$. The polarization curves were obtained in duplicate experiments with estimated error of ~10% afted 2 h to reach the stationary state. Impedance spectroscopy measurements were performed *in operando* in the 10^4 to 10^{-1} Hz *f*-range with potential amplitude of 5 - 10 mV.

3. Results and discussion

3.1. Ex situ conductivity with in-plane in 2- and 4-probes

3.1.1. Impedance spectra analysis

In Fig. 2, the 2 and 4-probe impedance spectroscopy measurements in the in-plane setup, as previously reported by Simonsson et al. [4] and Wainright et al. [5], were reproduced. In Fig. 2a and b, according to Simonsson et al. and Wainright et al., the *dc* conductivity of Nafion in the 4-probe measurements can be obtained at zero phase angle and at the modulus plateau for $f < 10^5$ Hz, which would represent the total impedance modulus of the film. However, as indicated by a dotted line in Fig. 2a and b, the frequency range of the measurements performed by Simonsson et al. and Wainright et al. were limited ($f > 10^0$ Hz), inhibiting the proper identification of the additional impedance process existing for $f < 10^{-1}$ Hz. In the Bode plots of Fig. 2a, the 4-probe measurements reveals an additional dispersion process, as observed by the phase angle minimum at $f \sim 4 \times 10^{-1}$ Hz, which reaches zero phase angle at $f \sim 1 \times 10^{-1}$ Hz. Likewise, in Fig. 2b, the Bode plots evidence a second impedance modulus in the same frequency range.

The measurements of in-plane and 4-probe setups are performed with widely separated platinum wires (1 cm apart), and the impedance data are collected with internal electrodes free from the effects of electrode/ionomer interfacial polarization. Both features suppress the electric double layer (EDL) contributions at electrode/ionomer interface in the impedance spectra. Therefore, exempt from interfacial polarization effects, the resistance and capacitance accessed in the 4-probe setup are mainly a result of the mean free path for migration and the build-up of protonic charges, respectively, across the heterogeneous morphology of the ionomer [19]. As such, the total impedance of Nafion (N115) obtained at $f \sim 10^{-1}$ Hz represents the genuine *ac*-to-*dc* proton conductivity crossover, and the estimated conductivity is $\sigma \sim 0.03$ Scm^{-1} at $T = 80$ °C and $RH = 100\%$. It is worth

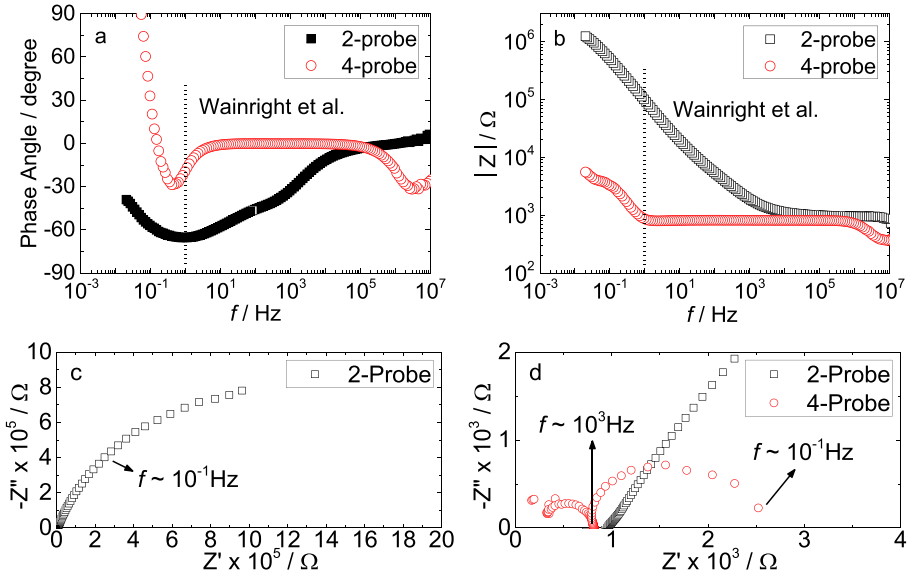

Fig. 2. Bode plots (*a* and *b*) and Nyquist plots (*c* and *d*) for Nafion membranes measured in the 2 and 4-probe in-plane setups at $T = 80$ °C and $RH = 100\%$. In (*a*) and (*b*), the short-dot line indicates the low frequency limit measured in the Wainright's work [5].

noting that the proton conductivity obtained with the high frequency intercept ($f \sim 10^3$ Hz) of the Nyquist plot of Fig. 2d is $\sigma \sim 0.10$ Scm^{-1} is similar to the conductivity obtained at the low frequency intercept ($\sigma \sim 0.03$ Scm^{-1}). Consequently, both values are similar to the conductivity values obtained in H_2/O_2 fuel cell polarization curves ($\sigma \sim 0.03$ to 0.05 Scm^{-1}), and, essentially, this feature is possibly the reason why detailed characterization of the impedance processes taking place at low frequencies is overlooked and hastily assigned uniquely to electrode polarization phenomena.

In Fig. 2d, the Nyquist plot of Nafion in the 4-probe setup evidences two semicircles, in which the high frequency semicircle exhibits negligible depression and marks a resistance at $f \sim 10^3$ Hz. This high frequency semicircle is shown in detail in Fig. 3a. Such Debye-like high frequency semicircle is constantly reported for the measurements of ion-containing polymers [38,39,48]. However, this undepressed semicircle represents a proton conduction transport within a phase of high homogeneity, which is surely not the case for an ionomer membrane with at least two amorphous ionic/non-ionic and crystalline phases. Similarly to polycrystalline materials that the impedance spectra exhibit separate contributions arising from ion conduction processes within grain and grain boundary [41], the high frequency semicircle can possibly be assigned to the displacement of protons within a domain of short length scale. As shown in Fig. 3b, NMR measurements of Nafion reveal two distinct relaxation times for proton transport, which is in accordance with two well-defined resistances obtained in impedance spectroscopy (Fig. 2).

In NMR measurements of Fig. 3b, it is observed that at $RH = 100\%$ two peaks can be seen related to two populations of protons, the peak located at short relaxation times is linked to protons of low mobility, in close to proximity to sulfonic groups [30]. On the other hand, the peak located at longer relaxation times is related to protons farther from these sulfonic groups and located in the bulk of the hydrophilic channel, which have greater mobility [30].

By using the *dc* proton conductivity estimated in Fig. 2, the proton diffusion coefficient can be calculated using Nernst-Einstein relation [15]:

$$D = \frac{\sigma k_b T}{ne^2} \quad (2)$$

where k_b is the Boltzmann constant, T is the absolute temperature, e is the elementary charge, and n is the charge carrier concentration. At $T = 80$ °C and $RH = 100\%$, the estimated diffusion coefficient with the conductivity obtained at low frequency *ac*-to-*dc* crossover is $D \sim 5.21 \times 10^{-6}$ cm^2 s^{-1}, which is in good agreement with the values estimated by NMR [40]. As NMR measurements are performed in free-standing Nafion films, the diffusion coefficient would correspond mostly to the measurements without the interfacial effects (4-probe).

The diffusion coefficient obtained with the high frequency semicircle is $D \sim 1.74 \times 10^{-5}$ cm^2 s^{-1}. Considering the diffusion coefficient estimated at the high frequency conductivity, the length scale L for proton conduction can be calculated using the relaxation frequency, $f^{-1} = L^2/D$. In the in-plane and through-plane setups, the high frequency semicircle is usually observed for $f > 10^3$ and $> 10^6$ Hz, and in such frequency ranges, the probed length scales correspond to $L < 16$ nm and $L < 0.5$ nm, respectively. Two phenomena can account for proton displacements at such short-length scales: *i)* protonic oscillations taking place in water domains; and *ii)* counterion fluctuations, *i.e*, the ion-hopping (forward-backward motion) of protons coordinated with the sulfonic groups compensating sites [53,54]. In short length scales, both processes would involve very homogeneous activation energies and consequently a Debye-like semicircle in the impedance spectra. In addition, the low frequency *dc* conductivity represents the proton motion coordinated with the sulfonic groups over long length scales. As coordinated with the sulfonic charges, the proton transport experiences the tortuous pathways across the ionomer nanophase heterogeneities in good accordance with the low frequency depressed semicircle.

It is worth of note that in both 2 and 4-probe impedance measurements a phase angle shift is observed (Fig. 2a) evidencing a relaxation process at $f \sim 4 \times 10^{-1}$ Hz, indicating that the interfacial polarization and sample bulk polarization are overlapped in the same frequency range. The lower conductivity values obtained with the 2-probe setup can possibly be linked to the interfacial polarization at the electrode/sample interface [20]. In previous reports, the logσ *vs* log$f$ plots of ionic liquids showed that due to strong interfacial polarization effects the formation of the *dc* conductivity plateau is hindered [20]. This characteristic was mainly associated with the largely reduced *dc* conductivity in the interfacial region since strong coulombic forces are experienced at the EDL inner and diffuse layers when E_c is higher than the thermal energy k_BT ($E_c \gg k_BT$). This is in perfect agreement with 2-probe (through-plane) measurements of Nafion as a function of temperature reported previously in which the formation of a *dc* conductivity plateau could be better defined with increasing temperature [15]. In the 2-probe setup, the conductivity obtained from the impedance modulus at low frequencies ($f \sim 10^{-2}$ Hz) of Fig. 2b is substantially reduced ($\sigma \sim 10^{-5}$ Scm^{-1}) compared to the 4-probe setup ($\sigma \sim 10^{-2}$ Scm^{-1}). In addition, in the 2-probe setup (Fig. 2a), the phase shift (-70°) observed at $f \sim 10^{-1}$ Hz tends to zero as the frequency decreases to $f \sim 10^{-2}$ Hz. Although the tendency of the phase angle of reaching zero indicates an onset of the *dc* conductivity in 2-probe setup, the absence of a plateau in the impedance modulus (Fig. 2b) shows that the interfacial polarization hinders the proper identification of the *dc* conductivity.

3.2. Ex situ conductivity with through-plane in 2- and 4-probes

3.2.1. Impedance spectra analysis

Fig. 4 shows the Nyquist plots for the 2 and 4-probe setups in the through-plane mode (Fig. 1) for Nafion. Similarly to the in-plane measurements shown in Fig. 2, in Fig. 4, it can be seen that the conductivity of Nafion in 4-probe setup (Fig. 4a) does not exhibit the large capacitive arc extending to low frequencies (Fig. 4b), assigned to electrode/ionomer interface. Likewise for in-plane measurements, the total impedance of Nafion is obtained at $f < 10^{-1}$ Hz, rather than at $f \sim 10^6$ Hz. In Fig. 4b, the Nyquist

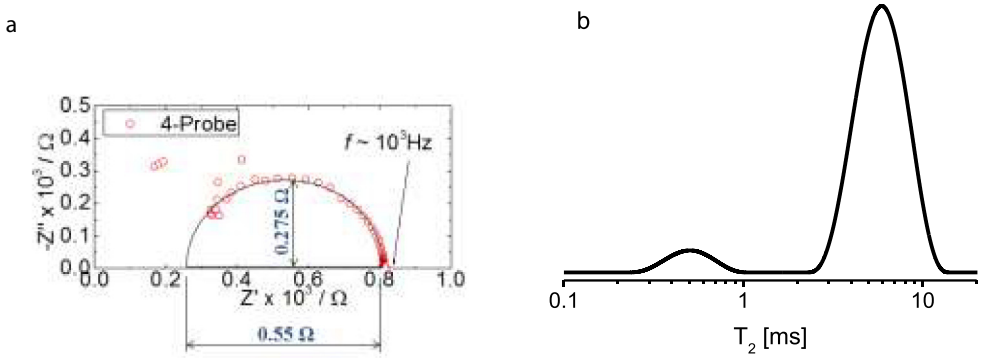

Fig. 3. (*a*) High frequency range of the Nyquist plots for Nafion measured in the 4-probe in-plane setups at $T = 80$ °C and $RH = 100\%$. (*b*) Water proton T_2 distribution profiles in Nafion at $T = 25$ °C and $RH = 100\%$.

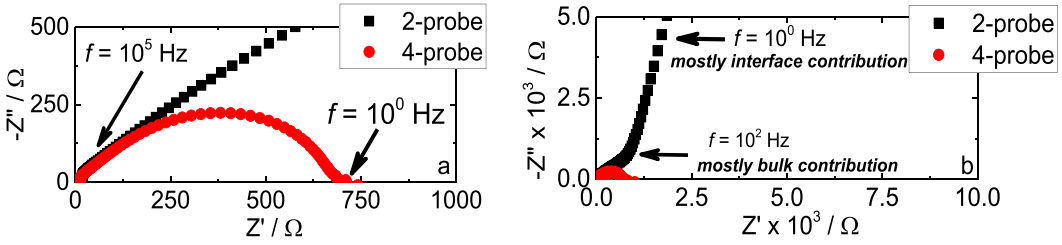

Fig. 4. Nyquist plots for Nafion at $T = 60$ °C and $RH = 100\%$ in the 2 and 4-probe through-plane setups exhibiting two different resistance windows (a and b).

plot shows major ionomer contributions at $f < 10^2$ Hz, while interfacial polarization contributions are clearly observed for $f > 10^2$ Hz. This feature is a further evidence that the ionomer electrical response is overlapped with the interfacial polarization in the low frequency semicircle. However, the *dc* proton conductivity as estimated from the low frequency intercept of the 4-probe impedance semicircle (Fig. 4a) is $\sigma \sim 3 \times 10^{-5}$ Scm^{-1}, which is 3 orders of magnitude lower than the 4-probe protonic conductivity measured in the in-plane setup (Fig. 2).

Possibly, even with four probes, considering the small sample thickness, electrode/ionomer interfacial polarization can still be present. In order to evaluate this effect, 2- and 4-probe conductivity in the through-plane setup was performed in samples with a different set of thicknesses. For 2-probe measurements, Nafion membranes with different ionomer thicknesses were prepared by casting (100 – 785 μm), and for the 4-probe measurements, different thicknesses were obtained by stacking up N115 membranes ($L \sim 160$ μm at $RH = 100\%$), as shown in Fig. 5. For minimizing electric field edge distortions, the thickness range was chosen considering the relation $L \square D^{1/2}$, where D is the diameter of the electrodes. The study of the thickness dependent conductivity by comparing a stack of

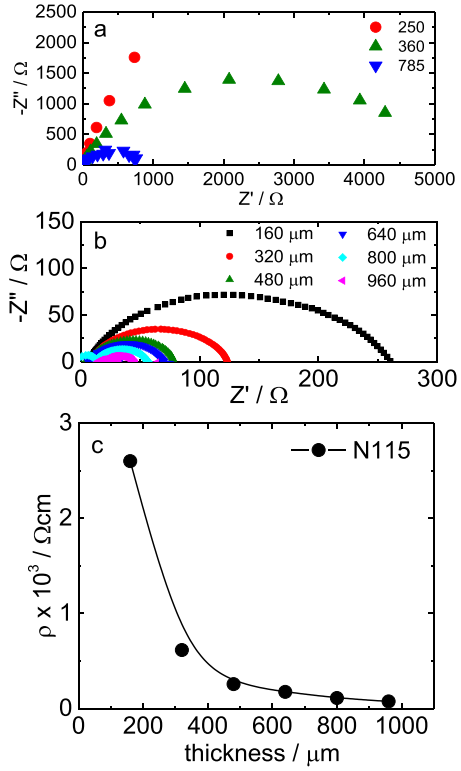

Fig. 5. Nyquist plots at $T = 130$ °C and $RH = 100\%$ in the 2-probe setup for Ncast films with different thicknesses (*a*); Nyquist plots at $T = 25$ °C and $RH = 100\%$ in the 4-probe setup for different stacks of N115 membranes (*b*); Protonic resistivity as a function of the distance between electrodes (N115 stacks) at $T = 25$ °C and $RH = 100\%$ in the 4-probe through-plane setup (*c*).

N115 and Ncast samples with different thicknesses is worthwhile for confirming that the changes in the proton conductivity is a feature occurring in the ionomer bulk, since the membrane surface interfaces due to stacking is eliminated in the samples prepared by casting.

In Fig. 5, the Nyquist plots for both 2 and 4-probe setups evidenced a marked decrease of the film resistance with increasing thickness. The dependence of the proton conductivity on thickness is a well-reported phenomena for Nafion [25,39,47], and such deviation from the ohmic behavior has been previously assigned either to a proton tunneling mechanism or to skin effects [25,47]. In Fig. 5a, the calculated conductivity increases from $\sigma \sim 10^{-6}$ to $\sigma \sim 10^{-5}$ and 10^{-4} Scm^{-1} by varying the thickness from 250, 360 and 785 μm, respectively. It is worth noting that this effect is pronounced for thickness larger than 250 μm, as the N112 (60 μm) and N115 films display similar conductivity than the 250 μm thick film. In the 4-probe setup (Fig. 5c), as the distance between the electrodes increases, a non-linear reduction of the resistance is observed resulting in a decrease of the proton resistivity reaching a plateau at ~ 75 Ω cm for 960 μm thick sample. In the 160 - 960 μm thickness range, the proton conductivity increased from $\sigma \sim 3.85 \times 10^{-4}$ to 1.13×10^{-2} Scm^{-1}, reaching the slightly lower values compared to the in-plane (4-probe) conductivity ($\sigma \sim 3 \times 10^{-2}$ Scm^{-1}). The 2- and 4-probe measurements in the through-plane setup confirm that the electrode/ionomer interfacial polarization affects the determination of the bulk conductivity. Moreover, the through-plane setup adds further evidence that the interfacial polarization occurring at the electrodes is the main factor associated with the non-linear increase of the proton conductivity with increasing thickness. It is possible to infer that as the membranes thickness increases, the ratio between the electrodes' separation (L) and the Debye screening length (λ) increases, and the proton conductivity approaches the bulk values. In addition, with increasing the electrodes' separation, the sample-holder capacitance decreases further reducing the interfacial polarization effects.

3.2.2. Dielectric spectra analysis

Similarly to the procedure performed in Figs. 2 and 4, the dielectric spectra of Nafion was studied in the 2- and 4-probe measurements in order to determine the dielectric permittivity values of Nafion with minimum electrode/ionomer interfacial polarization. Fig. 6 shows the dielectric spectra representation of the measurements performed in Fig. 5 for Nafion. In the Sup. Inf., the real and imaginary components of both dielectric and conductivity data are shown (Fig. S2) in order to ensure the correspondence between the *dc* conductivity as evaluated in the conductivity and dielectric spectra.

Fig. 6a shows the dielectric spectra of Nafion measured in the 2- and 4-probe setups at $T = 80$ °C and $RH = 100\%$. For both two and four probes, the dielectric constant increases with increasing membrane thickness. Moreover, the dielectric permittivity of the 4-probe measurements ($\varepsilon' \sim 10^6$ at $f = 10^2$ Hz) is lower compared to the 2-probe setup ($\varepsilon' \sim 10^8$ at $f = 10^2$ Hz). According to the theory of dielectric materials, as the distance between electrodes increases, the capacitance due to the induced surface charges in the dielectric layer at the electrode/ionomer interface decreases [19,37]. Therefore, the dielectric spectra of Nafion, exempt from interfacial electrode/ionomer, are obtained with the use of the 4-probe setup with samples with large thickness as shown in Fig. 6b. This measurement reveals

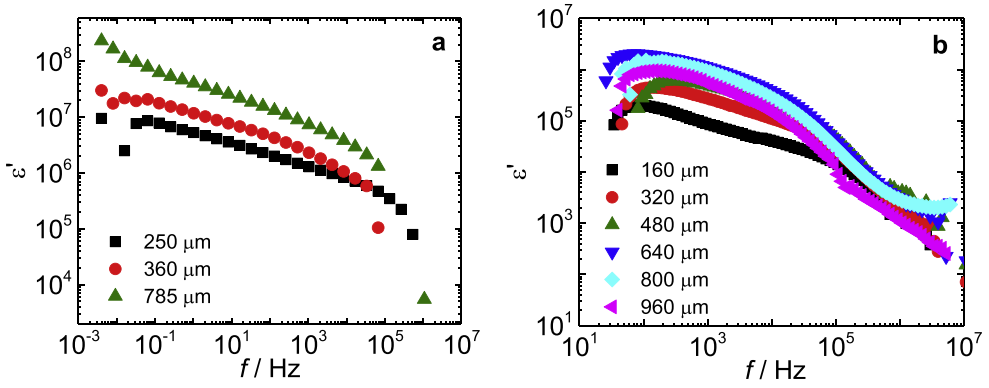

Fig. 6. Dielectric constant at $T = 80$ °C and $RH = 100\%$ in the 2-probe setup for Ncast membranes prepared with different thicknesses (*a*). Dielectric constant at $T = 25$ °C and $RH = 100\%$ in the 4-probe setup with different thicknesses for N115 by stacking up to 6 membranes (*b*).

that in the 10^{-1} - 10^{6} Hz *f*-range, the observed relaxations are polarization processes occurring in the polymer bulk, and that the measured colossal dielectric constant is an intrinsic property of the ionomer film. Moreover, the increase of the dielectric constant with increasing thickness can be evaluated by comparing Figs. 5 and 6, which evidences an increase of the dielectric constant with increasing proton conductivity. This trend between the conductivity and dielectric constant is commonly observed for polymer colloidal systems and is a signature of MWS polarization, reinforcing the view that the relaxations observed in the dielectric spectra are a result of the ionic polarization of Nafion building blocks [32,46].

The Debye length is strongly dependent on the dielectric constant of the medium. Typical Debye length is of the order of $\lambda \sim 1 - 100$ nm in a dilute aqueous medium with a dielectric constant of $\varepsilon' \sim 80$ [45]. The Debye length of EDL of the electrode/ionomer interface can be calculated by using the relation, $f^{-1} = \lambda^2/D$, in which the relaxation frequency is *ac*-to-*dc* crossover of the 2-probe measurements shown in Fig. S2 (Sup. Inf.) ($f \sim 10^{-3}$ Hz) [20,45,46], and the diffusion coefficient is equally obtained with the 2-probe *dc* proton conductivity ($\sigma \sim 2 \times 10^{-6}$ Scm^{-1}). Due to the low *ac*-to-*dc* frequency and extremely low diffusion coefficient, the calculated λ is in the micrometer range 16 μm ($2\lambda \sim 32$ μm). However, such formula is for a dilute electrolyte solution with a single relaxation time, which is not realistic for Nafion that displays at least two relaxation processes with elevated dielectric constant values.

In this context, a compound Debye length can be calculated considering the relaxation of the polymer phase located at the lowest frequency using the relation: $f^{-1} = (\lambda^2/L_p)f_p^{-1}$ [45,46]. As the proton is transported along the ionomer bulk, the protonic motion is restricted due to the potential well existing across the ionomer heterogeneities, and therefore, L_p (2.5 μm / Table 1) corresponds to the size or correlation length of such heterogeneities and f_p (0.03 Hz / Table 1) is the frequency at which such building blocks are polarized. This compound Debye length is reasoned considering that in polyelectrolytes there is a fraction of condensed counterions coordinated to the polymer chains, and free ions in solution, which give rise to the formation electric double layers in which the former is associated with the Stern layer, and the later with the diffuse layer [32,46]. The estimated Debye length is 76 μm ($2\lambda \sim 152$ μm). It is possible to infer that since the estimated thickness is comparable to Nafion's commercially available thicknesses (< 178 μm), the thickness dependent properties of Nafion are in agreement with the strong interfacial polarization effects due to the electrode/electrolyte interfaces, which promote a non-linear behavior when $\lambda \not\ll L$ [45,50]. In Fig. S3 (Sup. Inf.), the proton conductivity spectra are shown for Ncast samples with increasing thickness from 250 to 785 μm. And the proton conductivity spectrum of N112 (60 μm) is shown for comparison. The proton conductivities of both 60 and 250 μm thick membranes are similar ($\sigma \sim 10^{-6}$ Scm^{-1}), indicating that for thickness lower than 250 μm, the interfacial polarization spans over the entire membrane thickness reducing the proton conductivity. In addition, this feature is also in agreement with the 2-probe measurements in the through-plane setup in which the proton conductivity dependence on thickness was shown to be less accentuated for thickness larger than 250 μm.

According to the Debye screening length of EDL, the diffuse layer is dependent on the effective dielectric constant of the medium [45]:

$$\lambda = \sqrt{\frac{\varepsilon k_b T}{2z^2 e^2 n}} \tag{3}$$

Considering the colossal dielectric constant values seen in Fig. 6b, the accumulation of charges at the electrodes' surface is increased by ε', thereby by increasing ε' values from 10^3 to 10^6 units results in an increase of the Debye length from 295 μm to 9 mm! Such screening length is in good agreement with the reduction of the conductivity due to interfacial effects in the 2-probe for in-plane setups in which the proton conductivity is reduced ($\sigma \sim 10^{-5}$ S cm^{-1}) even for electrodes separated by 10 mm, as in Fig. 2. Previous studies on streaming potentials due to fluid flow in microchannels showed conductivity dependent on capillary size, when the capillary diameter is of the same order of magnitude compared to the Debye length [50]. It was concluded that the total (interfacial + bulk) conductivity becomes equal to the bulk conductivity when the channel width is infinitely large compared to the Debye length [50]. Such thick interfacial polarization indicates that the length scales being probed inside the polymer bulk spans over the entire length of the sample. This is possibly the reason why the interfacial polarization in 2-probe measurements as shown in Figs. 2 and 4 cover such a broad frequency range.

It is important to consider that in Eq. (3), the dielectric constant is usually taken as the dielectric constant of water. This is the case when the electrolyte placed between the two electrodes is a perfect conductor [37]. The dielectric constant of a perfect conductor is infinite, which means that the *dc* conductivity screens in totality (infinitely fast screening) the electrode's surface charges [37]. In this way, the only source of dielectric polarization in a parallel-plate capacitor in a dilute aqueous electrolyte would be the orientation of water around the electrode/electrolyte interface [37]. Therefore, the Gouy-Chapman model does not account for electrochemical systems containing ion-containing polymers that display elevated polarizability, *i.e*, the dielectric polarization due to the accumulation of charges across the polymeric interfaces. This reasoning can also be applied to ionic liquids due to the huge dielectric permittivity values found in those systems [20].

In this context, the interfacial features existing in the spectra obtained via 2-probe measurements is largely an outcome of the extra, and huge, amount of induced charge carriers added to the electrode's surface after the insertion of the Nafion film with colossal dielectric constant. The next section will deal with the origin of such giant dielectric constant of Nafion.

3.2.3. Phenomenological model

To provide a better insight into the effective polarization mechanism, Nafion membranes in the nonionic form were gradually converted to the

ionic form and the effects on the proton conductivity and dielectric constant are shown in Fig. 7.

In Fig. 7a and b, it can be observed that the both dielectric constant and proton conductivity are interchangeably connected. With decreasing *EW* from 42200 to 2900 g Eq^{-1}, the dielectric constant ranges from values observed for nonionic polymers ($\varepsilon' < 10$) to the ones observed for polymer with embedded water ($\varepsilon' \sim 80$), as shown in Fig. 7b [19]. Similarly, the proton conductivity increased linearly in this same *EW*-range from $\sigma \sim 3 \times 10^{-8}$ to 2×10^{-6} Scm^{-1} (Fig. 7a). Such increase of the proton conductivity can be accounted for the increase of the number of charge carriers [19,49]. However, a pronounced increase of the proton conductivity from $\sigma \sim 2 \times 10^{-6}$ to 6×10^{-5} Scm^{-1} is observed by increasing *EW* from 2900 to 1300 g Eq^{-1}. Within this *EW*, the ε'-values increased from 80 to 400. With further decreasing *EW* from 1300 to 1200 g Eq^{-1}, an abrupt boost of the proton conductivity from a semiconductor range ($\sigma \sim 6 \times 10^{-5}$ Scm^{-1}) to an elevated proton conductivity ($\sigma \sim 0.03$ Scm^{-1}) is observed. Likewise for ε'-values, the dielectric constant values with such small *EW* reduction increased from 400 to one million units.

The widely known mechanism that produces polymer dielectric dispersions of high dielectric polarizability is the MWS dispersion, which is associated with the contact between phases with different volume conductivities and dielectric permittivities [46]. The theory of MWS dielectric dispersion does not take into account any specific surface properties and is insensitive to the particle size [46]. MWS polarization can be a result of the polarization of either free or bound charges, difference of conductivities in hydrated and dry samples, and of dry phase segregation of distinct ion conductivities [46]. In this context, considering the broad *EW* range assessed, the increase of the dielectric constant with increasing *EW* from 2985 to 1279 g Eq^{-1} is possibly associated with the polarization at the boundary between ionic and nonionic domains by free ions in solution [55]. However, the abrupt rise of the dielectric permittivity over such small change in *EW* from 1300 to 1200 g Eq^{-1} can only be understood if detailed information on the distribution of the ionic charges within the ionomer phase is known. The large increment of the dielectric permittivity for $EW < 1300$ g Eq^{-1} suggests a criticality which can be accounted for by the counterion condensation theory [53]. Dielectric constant values of such magnitude are found for polyelectrolytes, when the polymer chains possess a linear ionic density higher than a critical value, satisfying the following equation: $n = zl_b / h > 1$; where h is the separation of monovalent charges z along the polymer chain is less than the Bjerrum length (l_b) [56]. In aqueous medium, the Bjerrum length is $l_b \sim 7$ Å, and suggests that with decreasing *EW*, as the sulfonate groups are gradually converted into sulfonic acid, the distance among them decreases until a distance lower than 7 Å is attained promoting the counterion condensation [56]. In such model, there is a distribution of ions free in solution and another distribution of condensed counterions, which are coordinated with sulfonate groups.

The Jonscher law is associated with the conduction of coordinated charges along the different length scales of the conductor phase experiencing a broad range of activation energies, which are dependent on the ion distribution along the sample [49]. In this scenario, the increase of the proton conductivity with increasing frequency, as shown in Fig. 7c, is a result of the forward and backward motion of ions coordinated to the sulfonic groups along the matrix heterogeneities. In Fig. 7c, it can be seen that with decreasing *EW* from 28300 to 1400 g Eq^{-1}, the high frequency portion ($f \sim 10^0$ to 10^6 Hz) of the conductivity spectrum rises, and the onset of the dispersive regime shifts to higher frequencies ($f \sim 10^{-1}$ to 10^1 Hz), respectively. The high-*f* shift of the onset is possibly a result of the decreasing distance among sulfonic acid groups with decreasing *EW*, which further decreases the activation energy for proton transport. Similarly, a catastrophic high-*f* shift of the onset of the dispersive regime with decreasing *EW* from 1400 to 1200 g Eq^{-1}, can be associated with a high linear charge density of the ionomer chains that promotes the condensation of counterions in the polymer phase thereby reducing abruptly the activation energies for proton transport. Such assignment is supported by the forward/backward displacement length of the protonic charges (~ 5 Å) as estimated from the high frequency intercept of the Nyquist plot (Fig. 4).

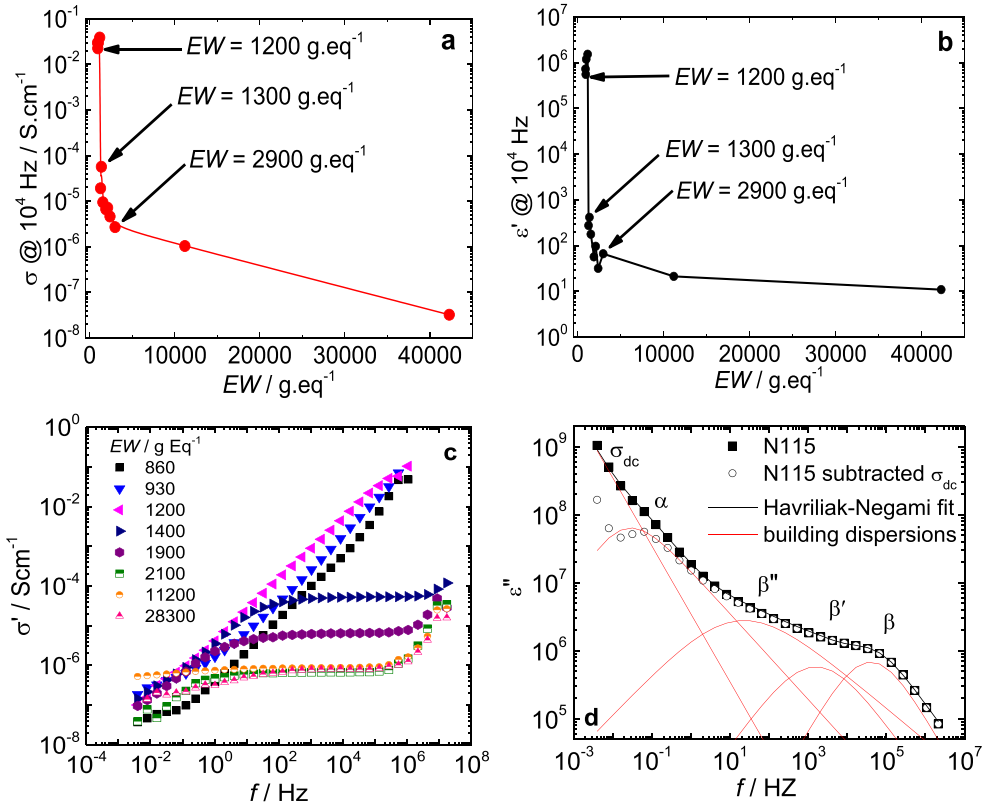

Fig. 7. (*a* and *b*) Proton conductivity and dielectric constant at $f = 10^4$ Hz for Nafion with increasing *EW*; (*c*) Frequency dependence of the real part of the conductivity for Nafion samples with increasing *EW*. (*d*) Havriliak-Negami fitting of Nafion dielectric loss spectrum at $T = 80$ °C and $RH = 100\%$.

Under the influence of an electric field, the condensed counterions diffuse along the length scales of the polymer chains, polarizing the building blocks of the polymer microstructure, which acts as induced microdipoles of elevated polarizability [53,56]. In polyelectrolyte science, such processes are observed in the dielectric spectra as a high and a low frequency relaxations, associated with the radial and longitudinal polarizations of the polymeric chains, respectively, and are observed in the frequency range of $f \sim 10^{-1}$ to 10^{6} Hz [53,54,56].

In order to determine the length scales of the polarizations within the ionomer building blocks, Nafion spectrum was fitted with the Havriliaki-Negami equation (Eq. (4)), as shown in Fig. 7d, and the corresponding fitting parameters and the estimated lengths are shown in Table 1.

$$\varepsilon^* = \varepsilon' - i\varepsilon'' = -i\left(\frac{\sigma_{dc}}{\varepsilon_0 \omega}\right)^n + \sum_{k=1}^{j}\left[\varepsilon_{\infty k} + \frac{\varepsilon_k}{(1+(i\omega\tau_{HN})^{\varphi_k})^{\gamma_k}}\right] \quad (4)$$

$$\tau_{max} = \tau_{HN}\left[\frac{sin\left(\frac{\pi\varphi\gamma}{2(\gamma+1)}\right)}{sin\left(\frac{\pi\varphi}{2(\gamma+1)}\right)}\right]^{\frac{1}{\varphi}} \quad (5)$$

where ω is the angular frequency ($\omega = 2\pi f$), $\Delta\varepsilon$ is the dielectric strength ($\varepsilon_0 - \varepsilon_\infty$); τ is the relaxation time given by Eq. (5), and the coefficients φ ($0 < \varphi < 1$) e γ ($0 < \gamma < 1$) stand for the width and relaxation asymmetry. Nafion dielectric spectrum is satisfactorily fitted considering the presence of at least 4 relaxation processes with increasing frequency, labelled α, β″, β′ and β. The -1 slope of β-relaxation unequivocally distinguishes it as a Debye polarization, and the subtraction of the *dc* conductivity reveals α-relaxation at low frequencies. The β″ has been observed previously for Nafion 105 (1000 g Eq^{-1}) [51]. In Table 1, the lengths associated with each relaxation is estimated using $f^{-1} = L^2/D$.

The estimated length scales are in excellent agreement with the ones estimated by SAXS and AFM as shown in Fig. S3 of the Sup. Inf.. In Fig. S3a, the SAXS plots of Nafion in the dry form displays the two scattering maxima located at $q \sim 2$ nm^{-1} and $q \sim 0.5$ nm^{-1}, which are attributed to the electronic contrast existing within the ionic and nonionic phases, with dimensions of ~ 3.14 and and ~ 12 nm, respectively [1]. In the hydrated form, the expansion of such domains changes its structural dimensions to ~ 5 and ~ 17 nm, respectively [57]. Previous ultra small-angle X-ray scattering of Nafion evidenced scaterring due to larger structures of the order of $L >$ 100 nm, which is possibly associated with the length of the polymeric aggregates [52]. The length scales probed by SAXS are in good agreement with the ones obtained by dielectric spectroscopy (Table 1). While the study of length scales larger than $L > 100$ nm is a hard task for SAXS, dielectric spectroscopy can assess very low frequency ranges and evaluate longer length scales. The lowest relaxation in the dielectric spectrum of Nafion is a result of a charge polarization within the length of ~ 2.5 μm. Accordingly, previous AFM images of Nafion topology reported heterogeneities on Nafion existing in the micrometer range [1]. Fig. S4b shows 2 × 2 μm^2 topography of Nafion surface measured by AFM in which a grooving pattern is observed vertically in the image. These vertically extended heterogeneities are observed with typical values of 1 μm and are in accordance with the values estimated in Table 1. The dielectric increment $\Delta\varepsilon$ of the longitudinal polarization was previously shown to be a function of the fraction of condensed counterions (1-θ), the counterion concentration (c), and the length of the polymer backbone (L) according to the relation, $\Delta\varepsilon \approx l_b e(1-\theta)cL^2$. Considering the estimated L values in the 1 – 2 μm range, the estimated dielectric increment ranges from $\Delta\varepsilon \sim 10^7$ to 10^8. Hence, the determination of the atypical proton conductivity and dielectric constant allows refining the morphological modelling and solve important open questions regarding the physical properties of Nafion such as dynamics of ion binding/unbinding and Donnan exclusion effects [17,33–36].

Table 1
Havriliak-Negami fitting parameters for compounding the experimental dielectric spectrum of Fig. 7d.

N115	τ_{max}/s	L/nm
α (γ = 0.9; φ = 0.70)	3.3 × 10^{1}	2500
β″ (γ = 0.8; φ = 0.60)	3.6 × 10^{-2}	90
β′ (γ = 1; φ = 0.80)	5.7 × 10^{-4}	12
β (γ = 1; φ = 1)	2.4 × 10^{-5}	2 - 3

3.3. In situ conductivity with through-plane in 2-probe

3.3.1. Ohmic regime

The characterization of the proton conductivity of ionomers in the 2-probe and through-plane setup is highly desirable because it represents more faithfully the membrane electrode assembly for electrochemical applications, such as capacitors, batteries and fuel cells. Initially, for simplicity, the impedance, conductivity and dielectric representations shown in Fig. 8 will be compared with the fuel cell polarization curve at the linear ohmic region, since there is a well-documented consensus of interpretation. Such comparison will help understanding the non-ohmic behavior of the proton transport that will be discussed in the next section (Fig. 9). It is worth emphasizing that the polarization curves were measured above the gas feed stoichiometry values and at ideal relative humidity conditions for avoiding concentration polarization processes that could result in additional impedance processes, which would hinder an unequivocal assignment of the relation between the proton transport and the fuel cell performance [44].

Fig. 8a and b shows the Nyquist plots of a PEFC operating at $T = 80$ °C and $RH = 100\%$ with N115 and N112, respectively. Fig. 8c and d shows the Nyquist plots for the ohmic region of the polarization curve at the indicated potentials. Fig. 8d and e shows the fuel cell electric data in the conductivity spectra representation (real part of the conductivity as a function of frequency). And finally, Fig. 8g and h shows the fuel cell electric data in the dielectric spectra representation.

In Fig. 8a and b, the Nyquist plots for the fuel cell show a single depressed semicircle in the frequency range of 10^0 to 10^4 Hz, exhibiting the typical reduction of the resistance with increasing overpotential ($E_{eq} - E$) [44]. In Fig. 8c and d, a magnification of the smaller semicircles is shown in the potential range that corresponds to the ohmic region of the polarization curves ($E < 800$ mV), which are shown in the insets of Fig. 8e and f. Fig. 8e and f shows the real conductivity spectra evidencing the increase of the low frequency conductivity plateau with increasing fuel cell overpotential. The conductivity plateau is highly dependent on potential at low current densities ($i < 100$ $mAcm^2$) and is weakly dependent on potential at the ohmic region (intermediate current densities / $i > 100$ $mAcm^2$), representing a transition of the non-linear to a linear regime. At $E = 0.73$ V for N115 (Fig. 8e) and at $E < 0.75$ V (Fig. 8f) for N112, the conductivity are σ ~ 0.030 Scm^{-1} and σ ~ 0.025 Scm^{-1}, respectively. The marked increase of the conductivity is detected as a high frequency shift of the *dc* conductivity slope in the dielectric loss plots, as observed in Fig. 8g and h.

In the ohmic region of the polarization curve, the rate determining step for the energy conversion is the proton conductivity within the ionomer phase. As the rate determining step, the proton conduction is consequently the slower process taking place in the fuel cell, *i.e.*, with the longest *RC* time constant [58]. Therefore, the low frequency depressed semicircle in the Nyquist plots of Fig. 8c and d corresponds to the charge transport and accumulation within Nafion heterogeneities, in accordance with the spectral analysis of Fig. 3. Moreover, the *dc* conductivity as identified in the fuel cell electric spectra in different representations (Fig. 8), *i.e.*, the low frequency intercept of the semicircle (Fig. 8a–d), the low frequency conductivity plateau in the conductivity spectra (Fig. 8e and f), and the low frequency *dc* conductivity slope in the dielectric spectra (Fig. 8g and h) matches perfectly with the blocking electrodes measurements, thereby revealing that the *ac*-to-*dc* crossover of proton conduction of Nafion in the fuel cell impedance curve is obtained for $f < 10^0$ Hz. This assignment is confirmed by comparing the proton conductivity as calculated from the polarization curve

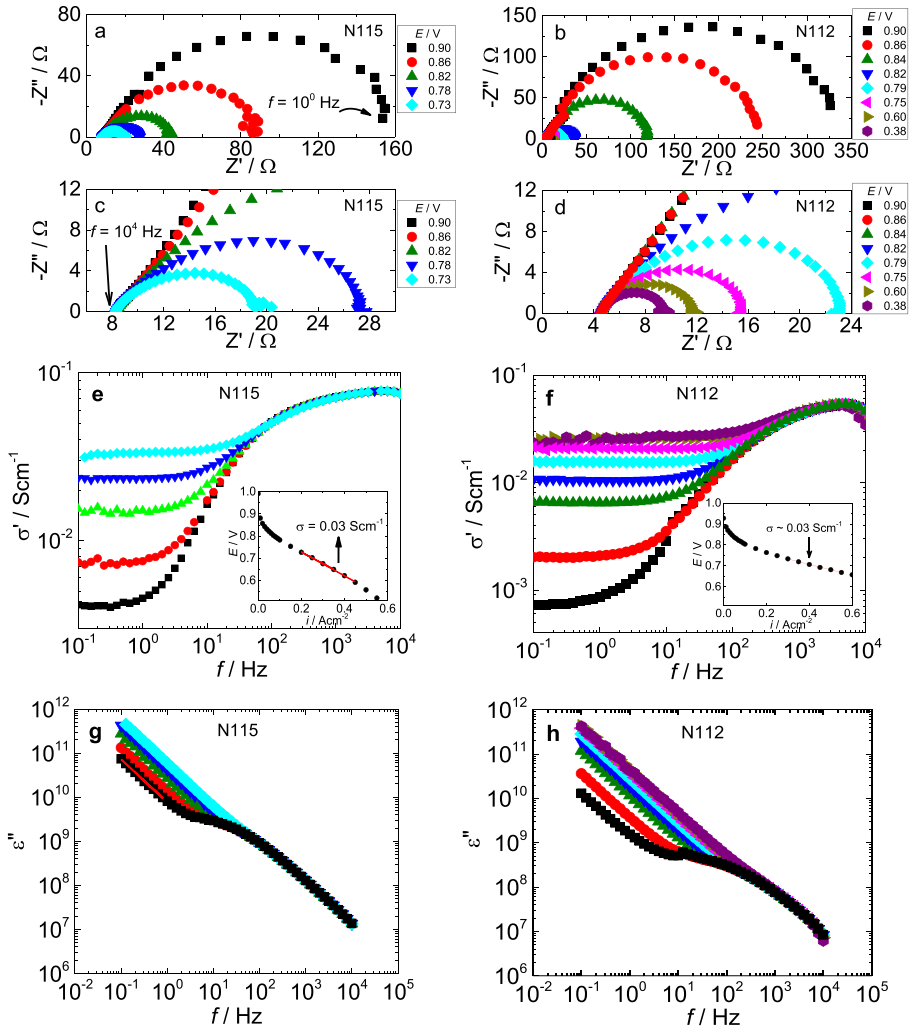

Fig. 8. (*a* and *b*) Impedance spectra for the PEFC at $T = 80$ °C and $RH = 100\%$ with decreasing potential for N115 and N112, respectively; (*c* and *d*) Magnification of the high frequency regions of the impedance spectra of (*a* and *b*); (*e* and *f*) Conductivity (real part) and (*g* and *h*) dielectric representations (imaginary part) of the impedance spectra shown in (*a*) and (*b*); the insets in (*e*) and (*f*) show the polarization curve and the estimative of the conductivity from the ohmic region slope.

slope (inset of Fig. 8e and f) with the values obtained in the low frequency conductivity plateau of Fig. 8e and f, which results rigorously in the same value $\sigma \sim 0.03$ Scm^{-1} ($T = 80$ °C and $RH = 100\%$). Such proton conductivity values are also in very good agreement which the ones obtained in Fig. 2 ($\sigma \sim 0.03$ Scm^{-1} at $T = 80$ °C and $RH = 100\%$). As such, the identification of the genuine *ac*-to-*dc* conductivity crossover of Nafion under fuel cell operation inevitably leads to a reinterpretation of the fuel cell impedance spectrum. The current interpretation of the impedance spectrum of a Nafion fuel cell supports that the *ac*-to-*dc* conductivity crossover due to the electrolyte conductivity takes place at high frequencies ($f \sim 10^4$ Hz), which is indicated by the arrow in Fig. 8c. The high frequency intercept of the fuel cell impedance cannot be assigned to the *dc* conductivity of Nafion since at $f \sim 10^4$ Hz the protonic charges displace at short-length scales not reaching the electrodes' surface. In addition, the low frequency intercept is assigned to the charge transfer due to redox reactions, which similarly, cannot be the case since at the ohmic region, the proton conductivity is the rate determining step for energy conversion.

3.3.2. Non-ohmic regime

In order to evaluate the non-linear portion of the polarization curve at low current densities in the same framework of Fig. 8, Fig. 9 shows the non-ohmic behavior of the proton conductivity of Nafion with applied *dc* bias. Specifically, a comparison of the potential dependent proton conductivity as estimated using blocking (Fig. 9a) and non-blocking (Fig. 9b) electrodes. Fig. 9c shows a schematic representation of the mechanism proposed for the potential dependent conduction behavior of Nafion.

Fig. 9a shows that the measured resistance decreases with increasing *dc* bias using blocking electrodes. In Fig. 9a, it can also be seen that the non-ohmic behavior of the resistance is accentuated at a potential difference ($\Delta E = E - E_0$) lower than 500 mV, whereas for $\Delta E > 500$ mV the resistance is nearly constant. Within the $\Delta E = 1100$ mV, the apparent proton conductivity increased from $\sigma \sim 6 \times 10^{-5}$ to 2×10^{-3} Scm^{-1}. For $\Delta E > 500$ mV, there is a change of slope of the apparent conductivity evidencing a transition to a regime of weaker dependence on potential. This finding is in accordance with previous reports that evidenced a critical potential difference ($\Delta E = 600$ mV) separating non-ohmic and ohmic regimes in Nafion proton conductivity, which within the total potential difference investigated ($\Delta E = 1200$ mV) the proton conductivity increased from $\sigma \sim 1 \times 10^{-4}$ to 4×10^{-3} Scm^{-1}, in good agreement with this study [25].

Fig. 9b shows the conductivity dependence on potential for the fuel cell operating with N115 and N112, obtained in the conductivity plots of Fig. 8. The graphs obtained for the blocking (Fig. 9a) and non-blocking (Fig. 9b) measurements are mirrored with each other as what is being confronted are the potential difference ($E - E_0$) with fuel cell overpotential ($E_{eq} - E$), respectively.

At $E = 0.90$ V (close to OCP), the proton conductivity of N112, for example, is $\sigma \sim 7.3 \times 10^{-4}$ Scm^{-1}. Close to OCP, the fuel cell system approaches the proton conductivity of the 2-probe setup with blocking

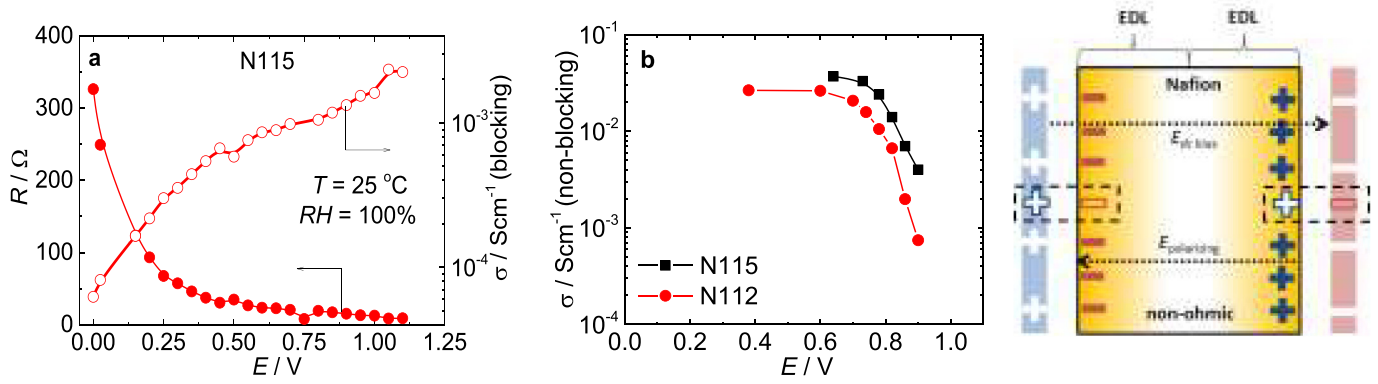

Fig. 9. Potential dependence of the Nafion membrane resistance and conductivity (T = 25 °C and RH = 100%) using blocking electrodes (*a*); Potential dependence of the N112 and N115 conductivity (T = 80 °C and RH = 100%) using non-blocking electrodes (*b*); Schematic representation of the mechanism associated with potential dependent conductivity (*c*).

electrodes (N112 / σ ~ 6.0 × 10^{-5} Scm^{-1}). With decreasing the fuel cell potential to E = 0.60 V, the proton conductivity is increased to σ ~ 2.5 × 10^{-2} Scm^{-1}. Similarly to the measurements using blocking electrodes, the potential dependence of the proton conductivity using non-blocking electrodes exhibits a non-ohmic behavior within a potential range of 0.60 – 1.0 V. As such, it can be inferred that an overpotential of 400 mV has to be supplied to attain the ohmic regime of higher conductivity, which is very similar to the potential difference (500 mV) observed in Fig. 9a.

The most important feature resulting from the comparison of the potential dependent conductivity with the use of blocking and non-blocking electrodes is that the close match between the potential difference values to promote a transition of the non-linear to the linear behavior using both systems suggests that the non-ohmic proton conduction of Nafion are not associated with charge transfer reactions on the electrodes. In addition, the overpotential as estimated from the blocking (500 mV) and non-blocking (400 mV) the non-ohmic conductivity plays a crucial role at low current densities in a fuel cell operation. This finding is highlighted in Vayenas' previous work: "*This non-linear conductivity dependence on cell potential can also describe the I–U characteristics of PEM fuel cells…*" [59]. The mechanism for the non-ohmic behavior of the conductivity observed in fuel cells can, therefore, be understood considering the scheme of Fig. 9c.

In a blocking electrodes's system, the insertion of a dielectric material between parallel plates under an electric field (and disconnected from the *dc* source) promotes a polarization of the dielectric [19]. As a consequence, the polarizing displacement field increases the capacitance ($C = \varepsilon C_0$) and reduces the electrodes' voltage ($E = E/\varepsilon$). In addition, the dielectric gives rise to intense electrostatic attraction between the dielectric layer and the electrode layer at the interface, thereby creating the interfacial polarization between ionomer and the charged plates. Such electrostatic energy reduces significantly the mobility of protons at the interface, and consequently, the proton conductivity. However, in 2-probe measurements with applied *dc* bias, such impedance measurements are equivalent to connecting the 2-probe sample-holder to a battery, where the potential difference is maintained constant at the battery terminal voltage. Therefore, with increasing *dc* bias, there will be an increase of the charge density at the sample-holder plates. Such incoming charges neutralize the induced opposing charges in the dielectric layer, thereby reducing the interfacial polarization and, consequently, promoting the transition of the proton conductivity from the non-ohmic to the ohmic regime (Fig. 9c).

In the fuel cell, however, such compensating potential is developed by triggering redox reactions in order to increase the number of charges to the capacitor plates and maintain the fuel cell equilibrium potential. In detail, the scheme of Fig. 9c for a PEFC using Nafion should be described as follows: the fuel cell anode is charged with H^+ and the cathode with electrons created by the hydrogen oxidation reaction; and the addition of a dielectric to the fuel cell electrodes increases the fuel cell electrodes capacitance. The energy spent in the electrostatic interactions between the charged plates and the dielectric reduces the total stored energy, which is the energy of polarizing the induced charges within Nafion film [19]. Therefore, such energy reduction represents a performance penalty to the fuel cell that must be overcome with an extra overpotential. In this way, the reduction of the interfacial polarization takes place when new H^+ charges are produced at the anode and the electrons are transported to the cathode via external circuit. However, the maintenance of the minimization of the interfacial polarization is dependent on rate of H_2O formation and removal from the cathode, which in turn are dependent on the slow kinetics of the oxygen reduction reaction.

However, one may ask, what is the rate determining step at low current density exponential decay in the fuel cell considering both the charge transfer and the non-ohmic proton transport? In the traditional interpretation of the fuel cell polarization curve, the transition from the activation polarization (low current density) to the ohmic drop (intermediate current density) should be identified in the Nyquist plots as a high frequency semicircle associated with ohmic transport and a low frequency semicircle due to charge transfer. With increasing current density from low to intermediate values, such semicircles should swap positions, since the ohmic transport becomes the slower process and its semicircle must be observed at the lowest frequency range. Such behavior is not evident in Fig. 8, at which in the impedance, conductivity and dielectric representations of the fuel cell data, the *dc* conductivity is represented by the same single semicircle in the non-linear and linear portions of the polarization curve.

According to the measurements with blocking electrodes shown in Fig. 9a and b, the observed semicircle is mainly a result of two convolved and inextricable *RC* constants due to the polarization of charges in Nafion bulk and the polarization at the ionomer/electrode interface. Both the frequency ranges of the ionomer response and interfacial polarization are similar (10^6 Hz > f > 10^{-1} Hz). Such similarity is reasonable since the charging of the electrode/ionomer interface is dependent on charging the ionomer microstructure. Therefore, the impossibility of separating the mutually dependent *RC* constants is due to the bulk and interfacial polarization to correspond to a single process: the proton conductivity. Therefore, the exponential decay of the polarization curve is marked by the elimination of the interfacial polarization by the charge transfer reactions.

It is reasonable to infer that if the proton conductivity is the slower process in the non-ohmic region; the proton conductivity is much slower at low current densities, as discussed in Figs. 2 and 3. A strong evidence supporting this assignment is the increase of the frequency of the *ac*-to-*dc* crossover with increasing current density. In Fig. 8g, with decreasing the fuel cell potential from 0.90 V to 0.38 V, the *ac*-to-*dc* crossover frequency increased from 10^0 to 10^2 Hz. In addition, under no *dc* bias (close to open circuit voltage), the *ac*-to-*dc* crossover frequency ranges from 10^{-2} to 10^{-3} Hz (Fig. S2). Therefore, from the non-ohmic to the ohmic regime, the *ac*-to-*dc* crossover frequency of Nafion increases by at least 4 orders of magnitude, reinforcing the view that the slow proton motion in Nafion at low

current densities may be the rate determining step associated with the exponential decay of the potential with increasing current density.

It is important to consider that the thickness dependent conductivity of Nafion is diametrically opposed to the effects associated with the electroosmotic drag of water. In the former, the proton conductivity of Nafion is lower the thinner the membrane is. In the latter, the anode drying due to electroosmotic drag is more accentuated for thicker membranes, resulting in lower overall proton conductivity [42,43]. Moreover, the conductivity behavior of both N115 and N112 are very similar indicating that the electroosmotic drag of water plays a minor role in the non-ohmic behavior of the proton conductivity [42,43]. Büchi et. al and Watanabe et. al observed that Nafion membrane resistance is dependent on the fuel cell current density and the results were associated with the electroosmotic dehydration of the membrane [42,43]. In Büchi's work, by stacking commercial Nafion membranes (60 – 400 μm), the electroosmotic drag of water was maximized promoting an increase of the membrane resistance in the anode side with increasing fuel cell current density [42]. In Fig. 9, the electroosmitic drag of water is minimized with the use of thin Nafion membranes (N112), which indicates that the electroosmotic drag of water cannot account for the non-ohmic conductivity of Nafion. On the other hand, the investigation of thin Nafion films 20-57 μm, Watanabe et al. reached an opposite result: the membrane resistance decreases with increasing current density [43]. It was shown that although electroosmotic drag plays a role in the conduction behavior of the membrane, the membrane resistance dependence on current density was mostly observed at both anode and cathode interfaces; and the ohmic resistance in the membrane bulk farther away from such interfaces is nearly independent on the current density [43]. This finding is in accordance with the results shown in Fig. 9, which indicates that the membrane resistance dependence on the current density is possibly associated with the interfacial polarization at the ionomer/electrode.

4. Conclusion

In this work, emphasis is given to the mismatch existing in the interpretation of the electric data of Nafion in different representations, such as impedance and dielectric spectra, which represents a problem to the advancement of the membrane and fuel cell science. Impedance/dielectric spectroscopy measurements with suitable instrumentation and characterization parameters allowed identifying the genuine *ac*-to-*dc* conductivity crossover frequency for perfluorinated sulfonic-acid ionomers membranes (PFSAs). By minimizing electrode/ionomer interfacial polarization effects using 4-probe electrodes (through-plane), the *ac*-to-*dc* crossover of Nafion was identified for $f < 10^{-1}$ Hz ($T = 40$ °C and $RH = 100\%$). In general, the 4-probe (in-plane) setup offers the most reliable method for obtaining the proton conductivity with minimum influence of electrode/ionomer interfacial effects. In addition, the 4-probe setup provides more realistic values compared to the ones obtained in fuel cells ($\sigma \sim 0.03$ Scm^{-1} at $T = 80$ °C and $RH = 100\%$), resulting in an electrolyte conductivity within $\sigma \sim 0.02 – 0.04$ Scm^{-1} ($T = 80$ °C and $RH = 100\%$). However, the determination of the bulk conductivity does not change the fact the proton conductivity of Nafion in the 2-probe setup is strongly reduced ($\sigma \sim 10^{-6}$ Scm^{-1}) due to interfacial polarization effects, which arises as a result of the giant dielectric permittivity of Nafion: $\varepsilon' \sim 10^6$ units. The giant dielectric permittivity is possibly a result of the polarization of condensed counterions along the nano-to-micrometer sized length scales within the ionomer phase, which acts as microdipoles, increasing in several orders of magnitude the dielectric permittivity. In order to consider the dielectric effects arising from the electrolyte, the interpretation of the fuel cell impedance/dielectric data was revisited. In single fuel cells, a non-ohmic to ohmic transition of Nafion proton transport takes place maximizing the proton conductivity under a potential difference of 400 - 500 mV. In this framework, such large dielectric polarization represents an additional polarization cost to the fuel cell performance and must be considered in the design of novel ionomer materials. The phenomenological model proposed in this work allowed accounting for most of the atypical properties of Nafion as well as the discrepancies existing between the impedance and dielectric spectra analysis of Nafion, without any apparent contradictions.

Declaration of Competing Interest

The author declare that they have no known competing financial interests or personal relationships that could have appeared to influence the work reported in this paper.

Acknowledgments

This work is dedicated to the memory of Prof. E. R. Gonzalez for the advice on studying the non-ohmic conductivity in Nafion. Thanks are due to Prof. T. Zawodzinski for the fruitful discussions. Thanks are due also to HZB (L. Puskar and U. Schade) and the LNLS (20160239) for the allocation of synchrotron radiation beamtime. H. Andrada (NMR), B. Tosco (AFM) and V. Andrea (PEM fuel cell tests). J. S. da Silva (EW membranes). And Capes.

Appendix A. Supplementary data

Supplementary data to this article can be found online at https://doi.org/10.1016/j.jelechem.2020.114357.

References

[1] A. Kusoglu, A.Z. Weber, New insights into perfluorinated sulfonic-acid ionomers, Chem. Rev. 117 (2017) 987–1104.
[2] G. Pourcelly, A. Oikonomou, C. Gavach, H.D. Hurwitz, Influence of the water content on the kinetics of counter-ion transport in perfluorosulphonic membranes, J. Electroanal. Chem 287 (1990) 43–59.
[3] J.J. Fontanella, M.G. McLin, M.C. Wintersgill, J.P. Calame, S.G. Greenbaum, Electrical impedance studies of acid form NAFION membranes, Solid State Ionics 66 (1993) l–4.
[4] B.D. Cahan, J.S. Wainright, AC impedance investigations of proton conduction in Nafion™, J. Electrochem. Soc. 140 (1993) L185.
[5] Y. Sone, P. Ekdunge, D. Simonsson, Proton conductivity of Nafion 117 as measured by a four-electrode AC impedance method, J. Electrochem. Soc. 143 (1996) 1254–1259.
[6] S. Ma, Z. Siroma, H. Tanaka, anisotropic conductivity over in-plane and thickness directions in Nafion-117, J. Electrochem. Soc. 153 (2006) A2274–A2281.
[7] A. Kusoglu, K. Vezzù, G.A. Hegde, G. Nawn, A.R. Motz, H.N. Sarode, G.M. Haugen, Y. Yang, S. Seifert, M.A. Yandrasits, S. Hamrock, C.M. Maupin, A.Z. Weber, V. Di Noto, A.M. Herring, Transport and morphology of a proton exchange membrane based on a doubly functionalized perflourosulfonic imide side chain perflourinated polymer, Chem. Mater. 32 (2020) 38–59.
[8] K.A. Page, B.W. Rowe, K.A. Masser, A. Faraone, The effect of water content on chain dynamics in nafion membranes measured by neutron spin echo and dielectric spectroscopy, J. Polym. Sci. B 52 (2014) 624–632.
[9] I.M. Hodge, A. Eisenberg, Dielectric and mechanical relaxations in a Nafion precursor, Macromolecules 112 (1978) 289–293.
[10] S.C. Yeo, A. Eisenberg, Physical properties and supermolecular structure of perfluorinated ion-containing (nafion) polymers, J. Appl. Polym. Sci. 21 (1977) 875.
[11] K.A. Mauritz, R.-M. Fu, Dielectric relaxation studies of ion motions in electrolyte-containing perfluorosulfonate ionomers. 1. NaOH and NaCl systems, Macromolecules 21 (1988) 1324–1333.
[12] S.J. Osborn, M.K. Hassan, G.M. Divoux, D.W. Rhoades, K.A. Mauritz, R.B. Moore, Glass transition temperature of perfluorosulfonic acid ionomers, Macromolecules 40 (2007) 3886–3890.
[13] J.-H. Lin, R.H. Colby, Evolution of morphology, segmental dynamics, and conductivity in ionic liquid swollen short side chain perfluorosulfonate ionomer membranes, J. Polym. Sci. B 53 (2015) 1273–1280.
[14] B.R. Matos, E.I. Santiago, J.F.Q. Rey, F.C. Fonseca, Origin of α and β relaxations of Nafion, Phys. Rev. E 89 (2014), 052601. .
[15] B.R. Matos, E.I. Santiago, J.F.Q. Rey, C.H. Scuracchio, G.L. Mantovani, L.A. Hirano, F.C. Fonseca, *dc* Proton conductivity at low-frequency in Nafion conductivity spectrum probed by time-resolved SAXS measurements and impedance spectroscopy, J. Polym. Sci. B 53 (2015) 822.
[16] B.R. Matos, R. Politano, J.F.Q. Rey, D. Hermida-Merino, U. Schade, L. Puskar, F.C. Fonseca, Interplay of α/β-relaxation dynamics and the shape of ionomer building blocks, Sci. Rep. 8 (2018) 13441.
[17] M. Ghelichi, M.H. Eikerling, conformational properties of comb-like polyelectrolytes: a coarse-grained MD study, J. Phys. Chem. B 120 (2016) 2859–2867.
[18] A. Wohlfarth, J. Smiatek, K.-D. Kreuer, S. Takamuku, P. Jannasch, J. Maier, Proton dissociation of sulfonated polysulfones: influence of molecular structure and conformation, Macromolecules 48 (2015) 1134–1143.
[19] A. Schönhals, F. Kremer, in: F. Kremer, A. Schönhals (Eds.), Broadband Dielectric Spectroscopy, Springer Verlag, Berlin 2003, p. 59.
[20] A. Serghei, M. Tress, J.R. Sangoro, F. Kremer, Electrode polarization and charge transport at solid interfaces, Phys. Rev B 80 (2009) 184301.

[21] D.C. Sabarirajan, J. Liu, Y. Qi, A. Perego, A.T. Haug, I.V. Zenyuk, Determining proton transport in pseudo catalyst layers using hydrogen pump DC and AC techniques, J. Electrochem. Soc. 167 (2020), 084521. .
[22] B. Jadi, A.E. Guerraf, A. Kiss, A.E. Azrak, E.A. Bazzaoui, R. Wang, J.I. Martins, M. Bazzaoui, Analyses of scanning electrochemical microscopy and electrochemical impedance spectroscopy in direct methanol fuel cells: permeability resistance and proton conductivity of polyanilinemodified membrane, J. Solid State Electrochem. (2020) https://doi.org/10.1007/s10008-020-04659-2.
[23] T.A. Zawodzinski Jr., M. Neeman, L.O. Sillerud, S. Gottesfeld, Determination of water diffusion coefficients in perfluorosulfonate ionomeric membranes, J. Phys. Chem. 95 (1991) 6040–6044.
[24] C.G. Vayenas, M.N. Tsampas, A. Katsaounis, First principles analytical prediction of the conductivity of Nafion membranes, Electrochim. Acta 52 (2007) 2244–2256.
[25] M.N. Tsampas, A. Pikos, S. Brosda, A. Katsaounis, C.G. Vayenas, The effect of membrane thickness on the conductivity of Nafion, Electrochim. Acta 51 (2006) 2743–2755.
[26] B.R. Matos, J.S. da Silva, E.I. Santiago, D.F. Parra, D.J. Carastan, D.Z. de Florio, H.E. Andrada, A.C. Carreras, F.C. Fonseca, Proton and cesium conductivity in perfluorosulfonate ionomers at low and high relative humidity, Solid State Ionics 301 (2017) 86–94.
[27] R.S. Chen, J.P. Jayakody, S.G. Greenbaum, Y.S. Pak, G. Xu, M.G. McLin, J.J. Fontanella, Studies of water in nafion membranes using deuteron and oxygen-17 nuclear magnetic resonance, and dielectric relaxation techniques, J. Electrochem. Soc. 140 (1993) 889–895.
[28] A. Katsaounis, S. Balomenou, D. Tsiplakides, S. Brosda, S. Neophytides, C.G. Vayenas, Proton tunneling-induced bistability, oscillations and enhanced performance of PEM fuel cells, Appl. Catal. B 56 (2005) 251–258.
[29] L. Puskar, E. Ritter, U. Schade, M. Yandrasits, S.J. Hamrock, M. Schaberg, E.F. Aziz, Infrared dynamics study of thermally treated perfluoroimide acid proton exchange membranes, Phys. Chem. Chem. Phys. 19 (2017) 626–635.
[30] H. Andrada, M. Franzoni, A. Carreras, F. Vaca Chávez, Dynamics and spatial distribution of water in Nafion 117 membrane by NMR spin-spin relaxation, Int. J. Hydrog. Energy 43 (2018) 8936.
[31] W.F.G. Saleha, R. Ramesh, N. Nalajala, A. Chakraborty, B.P. Ladewig, M. Neergat, Broadband dielectric spectroscopy of Nafion-117,sulfonated polysulfone (sPSF) and sulfonated polyetherketone (sPEK) membranes, J. Appl. Polym, Sci. 134 (2017) https://doi.org/10.1002/APP.44790.
[32] M. Pollak, H.A. Pohl, Dielectric dispersion in some polymers and polyelectrolytes: A model, J. Chem. Phys. 63 (1975) 2980.
[33] A. Münchinger, K.-D. Kreuer, Selective ion transport through hydrated cation and anion exchange membranes I. The effect of specific interactions, J. Mem. Sci. 592 (10) (2019), 117372. .
[34] J. Peng, T.A. Zawodzinski, Describing ion exchange membrane-electrolyte interactions for high electrolyte concentrations used in electrochemical reactors, J. Mem. Sci. 593 (2020) 117340.
[35] K.M. Beers, D.T. Hallinan Jr., X. Wang, J.A. Pople, N.P. Balsara, Counterion condensation in Nafion, Macromolecules 44 (2011) 8866–8870.
[36] D.B. Spry, M.D. Fayer, Proton transfer and proton concentrations in protonated Nafion fuel cell membranes, J. Phys. Chem. B 113 (2009) 10210.
[37] J.O.M. Bockris, A.K.M. Reddy, M. Gamboa-Aldeco, Modern Electrochemistry, Kluwer Academic/Plenum Publishers, New York, 2000.
[38] C. Yin, J. Li, Y. Zhou, H. Zhang, P. Fang, C. He, Phase separation and development of proton transport pathways in metal oxide nanoparticle/Nafion composite membranes during water uptake, J. Phys. Chem. C 122 (2018) 9710–9717.
[39] Z. Xie, C. Song, B. Andreaus, T. Navessin, Z. Shi, J. Zhang, S. Holdcroft, Discrepancies in the measurement of ionic conductivity of PEMs using two- and four-probe AC impedance spectroscopy, J. Electrochem. Soc. 153 (2006) E173–E178.
[40] K.D. Kreuer, On the development of proton conducting polymer membranes for hydrogen and methanol fuel cells, J. Mem. Sci. 185 (2001) 29–39.
[41] M. Gerstl, E. Navickas, G. Friedbacher, F. Kubel, M. Ahrens, J. Fleig, The separation of grain and grain boundary impedance in thin yttria stabilized zirconia (YSZ) layers, Solid State Ionics 185 (2011) 32–41.
[42] F.N. Büchi, G.G. Scherer, Investigation of the transversal water profile in Nafion membranes in polymer electrolyte fuel cells, J. Electrochem. Soc. 148 (2001) A183–A188.
[43] M. Watanabe, H. Igarashi, H. Uchida, F. Hirasawa, Experimental analysis of water behavior in Nafion electrolyte underfuel cell operation, J. Electroanal. Chem. 399 (1995) 239–241.
[44] T.J.P. Freire, E.R. Gonzalez, Effect of membrane characteristics and humidification conditions on the impedance response of polymer electrolyte fuel cells, J. Electroanal. Chem. 503 (2001) 57–68.
[45] M.Z. Bazant, K. Thornton, A. Ajdari, Diffuse-charge dynamics in electrochemical systems, Phys. Rev. E 70 (2004), 021506. .
[46] S.-S. Dukhin, V.-N. Shilov, Kinetic aspects of electrochemistry of disperse systems. Part II. Induced dipole moment and the non-equilibrium double layer of a colloid particle, Adv. Colloid. Int. Sci. 13 (1980) 153–195.
[47] S. Slade, S.A. Campbell, T.R. Ralph, F.C. Walsh, Ionic conductivity of an extruded nafion 1100 EW series of membranes, J. Electrochem. Soc. 149 (2002) A1556–A1564.
[48] R. Yadav, P.S. Fedkiw, Analysis of EIS technique and Nafion 117 conductivity as a function of temperature and relative humidity, J. Electrochem. Soc. 159 (2012) B340–B346.
[49] J.C. Dyre, T.B. Schrøder, Universality of ac conduction in disordered solids, Rev. Mod. Phys. 72 (2000) 873–892.
[50] H. Ban, B. Lin, Z. Song, Effect of electrical double layer on electric conductivity and pressure drop in a pressure-driven microchannel flow, Biomicrofluidics 4 (2010), 014104. .
[51] B.R. Matos, E.I. Santiago, R. Muccillo, I.A. Velasco-Davalos, A. Ruediger, A.C. Tavares, F.C. Fonseca, Interplay between α-relaxation and morphology transition of perfluorosulfonate ionomer membranes, J. Power Sources 293 (2015) 859–867.
[52] G. Gebel, J. Lambard, Small-angle scattering study of water-swollen perfluorinated ionomer membranes, Macromolecules 30 (1997) 7914–7920.
[53] G.S. Manning, J. Ray, Fluctuations of counterions condensed on charged polymers, Langmuir 10 (1994) 962–966.
[54] J.A. Fornes, Fluctuation-dissipation theorem and the polarizability of rodlike polyelectrolytes: an electric circuit view, Phys. Rev. E 57 (1998) 2110.
[55] M. Samet, A. Kallel, A. Serghei, Polymer bilayers with enhanced dielectric permittivity and low dielectric losses by Maxwell–Wagner–Sillars interfacial polarization: characteristic frequencies and scaling laws, J. Appl. Polym. Sci. (2019)https://doi.org/10.1002/APP.47551.
[56] F. Bordi, C. Cametti, R.H. Colby, Dielectric spectroscopy and conductivity of polyelectrolyte solutions, J. Phys. 16 (2004), R1423. .
[57] J.H. Lee, G. Doo, S.H. Kwon, S. Choi, H.-T. Kim, S.G. Lee, Dispersion-solvent control of ionomer aggregation in a polymer electrolyte membrane fuel cell, Sci. Rep. 8 (2018) 10739.
[58] J. Bisquert, Theory of the impedance of charge transfer via surface states in dye-sensitized solar cells, J. Electroanal. Chem. 646 (2010) 43–51.